frontiers | Frontiers in Energy Research

TYPE Original Research
PUBLISHED 08 April 2024
DOI 10.3389/fenrg.2024.1296709

OPEN ACCESS

EDITED BY
Simona Liguori,
Clarkson University, United States

REVIEWED BY
Omid Jazani,
Clarkson University, United States
Siamak Hoseinzadeh,
Sapienza University of Rome, Italy

*CORRESPONDENCE
Meng Li,
✉ 18569896803@163.com

RECEIVED 19 September 2023
ACCEPTED 21 February 2024
PUBLISHED 08 April 2024

CITATION
Ji X, Li M, Li M and Han H (2024), Low-carbon optimal operation of the integrated energy system considering integrated demand response and oxygen-rich combustion capture technology.
Front. Energy Res. 12:1296709.
doi: 10.3389/fenrg.2024.1296709

Low-carbon optimal operation of the integrated energy system considering integrated demand response and oxygen-rich combustion capture technology

Xiu Ji[1], Meng Li[2]*, Meiyue Li[2] and Huanhuan Han[2]

[1]National Local Joint Engineering Research Center for Smart Distribution Grid Measurement and Control with Safety Operation Technology, Changchun Institute of Technology, Changchun, China, [2]Changchun Institute of Technology, Changchun, China

In view of the current operating constraints and environmental pollution problems of traditional units, in this article, oxygen-rich combustion capture technology is introduced to transform gas-fired units, demand response technology is used on the load side, the energy conversion equipment such as power-to-gas equipment is combined to form an integrated energy system, and then, a low-carbon optimization approach of the integrated energy system is proposed. First, the system architecture is constructed, and a model with an oxygen-rich combustion unit and integrated demand response is established. Second, a power-to-gas equipment model considering reaction waste heat utilization and oxygen recovery is established. Finally, a stepped carbon trading mechanism is introduced to establish a low-carbon economic scheduling model for the integrated energy system with the goal of minimizing the operating cost of the integrated energy system. The simulation results show that the total cost and carbon emissions of the integrated energy system are reduced by 6.44% and 44.24%, respectively, under this model. At the same time, the operation adjustment capability and the oxygen production efficiency of the internal units of the system are improved.

KEYWORDS

oxygen-rich combustion capture unit, demand response, integrated energy system, low carbon, carbon trading mechanism

1 Introduction

The issues of environmental pollution and energy shortage have accelerated the global development trend of low-carbon emission and clean energy. In order to achieve the grand development goal of "carbon peaking and carbon neutrality," the complementary and coordinated optimization of an integrated energy system (IES) has become a key technical direction for addressing the contradiction between energy supply and demand and

Abbreviations: IES, integrated energy system; LAES, liquid air energy storage; P2G, power-to-gas; PDR, price-based demand response; IDR, incentive-based demand response; DR, demand response; LNG, liquefied natural gas.

improving energy conversion capabilities. Research on its optimized operation has become a hot topic (Han et al., 2021).

At present, the main measures taken to achieve the low-carbon IES can be classified into two categories: policy, such as establishing carbon trading mechanisms, and technology, such as carbon capture technology and demand-side response technology. The low-carbon economic operation of the entire system can be achieved by coordinating the above two main measures.

Currently, the main research method for achieving low-carbon scheduling is to introduce carbon trading mechanisms into the IES. Qin et al. (2018) introduced carbon trading mechanisms into the electricity–gas–heat integrated energy system, which can be conducive to the low-carbon economic operation of the system, promoting the development of low-carbon units. Zhou et al. (2018) introduced carbon trading mechanisms into the IES, and the results showed that carbon trading mechanisms can effectively promote the consumption of new energy, improving the low-carbon and economic efficiency of the IES. Wang et al. (2019) used the life-cycle analysis method to analyze the carbon emissions generated by different energy chain migration and transformation processes in the IES. The results showed that reasonable planning of the carbon market can promote the low-carbon development of the IES.

In the above research, the carbon trading mechanism can only function on gas-fired units within the IES. As thermal power serves as the external supply base load of the IES, the carbon trading mechanism cannot be effectively optimized. Therefore, the coordination of technology and policy should be considered.

Lu et al. (2018) established a minimum coordination relationship model between the heat storage and release rate and the electric boiler power under the condition of extreme wind power consumption. The results showed the effectiveness of the heat storage and coordinated heating relationship between extreme wind power consumption and the electric boiler. Gao et al. (2019) introduced power-to-gas (P2G) carbon capture power plants into the IES. The results showed that power-to-gas-carbon capture power plants can effectively improve the absorption capacity of wind power and reduce system carbon emissions and operating costs. He et al. (2018) analyzed the flexible operation modes of carbon capture systems and P2G equipment in the IES. The results showed that the proposed model and flexible operation mode can effectively reduce carbon emissions and operating costs of integrated energy systems.

It is worth mentioning that currently, limited research exists on the introduction of carbon capture technology in the IES. Among them, some scholars have adopted post-combustion capture technology for the low-carbon transformation of gas turbines, but there are shortcomings such as a huge covering area for the equipment, weak capture capacity, and high capture cost, which are suitable for thermal power units (Liu et al., 2010). The pre-combustion capture technology requires significant modifications to the unit, resulting in low applicability. The oxygen-rich combustion capture technology combines the advantages of pre- and post-combustion capture technologies, with little impact on the power generation process of the units and strong carbon capture ability. However, it has high requirements for the cleanliness of the fuel itself and is suitable for gas-fired units, with good development prospects (Dai et al., 2023).

Current research at home and abroad is mainly focused on the economics and operating characteristics of oxygen-rich combustion technology. Gao et al. (2014) analyzed the impact of changes in unit operating parameters and different flue gas re-circulation methods on air separation oxygen generation equipment and gas capture equipment and then established a calculation model for the operating energy consumption of the related equipment. Cui et al. (2021) established a dynamic cycle model and a dynamic change model of flue gas composition for oxygen-rich combustion flue gas and analyzed the energy consumption of power plants at different oxygen concentrations in oxygen-rich combustion scenarios. Oboirien et al. (2014) analyzed the energy consumption and economic performance of oxygen-rich combustion equipment under different parameters. Koiwanit et al. (2014) established a full process model of the oxygen-rich combustion system and proposed a utilization plan for residual heat based on thermodynamic principles to improve the operational economy of the system. Zaharia et al. (2019), Yang et al. (2022), and Guo et al. (2023) conducted an economic analysis of the investment cost, operating cost, and CO_2 emission reduction cost of oxygen-rich combustion power plants.

With the continuous enrichment and expansion of resources on the demand side, considering only oxygen-rich combustion technology and carbon trading mechanisms cannot meet the needs of the low-carbon operation of the IES. At present, utilizing demand-side resources for carbon reduction has become a research hotspot, but most of it focuses on the demand-side resource interaction from the perspective of "electricity." Zhou et al. (2018) and Ji et al. (2022) introduced the "electricity price" demand response (DR) model into the IES, and the results showed that the proposed model can effectively reduce carbon emissions and operating costs of the IES. Cui et al. (2022) proposed a new carbon reduction mechanism for power systems, which guides users to actively respond and reduce carbon emissions from a "carbon perspective" (Zhou et al., 2018; Malehmirchegini et al., 2022). Overall, whether from the perspective of users or the system, demand response mechanisms can bring carbon reduction benefits.

In summary, this paper proposes an optimal operation scheduling model of the IES that considers integrated demand response and oxygen-rich combustion capture technology. The main contributions of this paper are as follows:

1. An oxygen-rich combustion technology is introduced to transform the gas-fired unit, and a model of the oxygen-rich combustion capture unit is established for solving the operational constraints and environmental pollution problems of traditional units within the IES.
2. An integrated demand response model of price and subsidy incentives is constructed based on the price elasticity matrix principle and response subsidy policy to provide full play to the adjustment ability of demand-side response resources.
3. A stepped carbon trading mechanism is proposed, the impact of the base price of the carbon trading mechanism on system costs and carbon emissions is discussed, and the low-carbon operation model of the IES considering the stepped carbon trading mechanism is constructed.

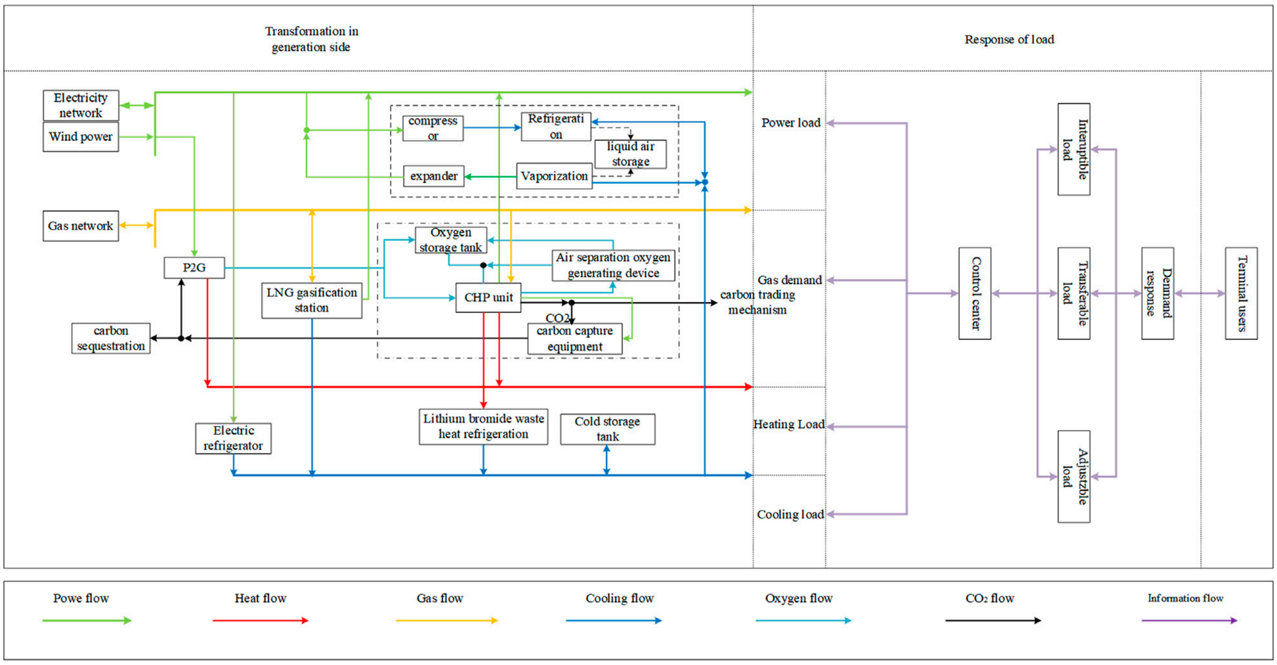

FIGURE 1
Integrated energy system structure.

2 Architecture of an integrated electricity–heat–gas-cooling energy system

The structure of the IES is shown in Figure 1. Here, the gas-fired unit adopts the oxygen-rich combustion capture technology for low-carbon transformation; electric power is supplied by the combined heat and power unit, wind power, and purchased electricity; the heat load is supplied by the combined heat and power unit and the residual heat from the P2G converter; the gas load is supplied by the external gas network and the P2G converter; the cold load is supplied by the air-conditioning and refrigeration, the residual heat from lithium bromide, and the liquefied natural gas tanks in the gasification process to supply the loads; and the oxygen required by the oxygen-rich combustion capture unit is supplied by the P2G converter, air oxygen generator, and oxygen storage tank. Oxygen for the oxygen-rich combustion capture unit is supplied by electric gas conversion equipment, air oxygen generating equipment, and oxygen storage tanks (Kang et al., 2022).

2.1 The modeling and combined heating-supply principle of the oxygen-rich combustion unit

2.1.1 Modeling of oxygen-rich combustion capture units

Oxygen-rich combustion capture technology increases the concentration of CO_2 in flue gas after combustion using high-purity oxygen or pure oxygen, which can be helpful for purification or storage after capture. The energy flow diagram of the oxygen-rich combustion unit is shown in Figure 2.

The main energy destinations of the oxygen-rich combustion capture unit are the system electrical load, carbon capture equipment, air separation oxygen generation equipment, and system heat load (Zhu et al., 2022).

Oxygen-rich combustion capture technology has a higher degree of fuel cleanliness, and back-pressure gas-fired units are selected as the object of transformation. The oxygen-rich combustion capture units in the following paragraph refer to the gas-fired units transformed by the oxygen-rich combustion capture technology. The relationship between electricity generation P_t^{GU} and natural gas consumption of a gas-fired unit V_t^{GU} is shown as follows:

$$\begin{aligned} &P_t^{GU} = \frac{V_t^{GU}\eta_{GU}L_{CH_4}}{r} \\ &P_{\min}^{GU} \le P_t^{GU} \le P_{\max}^{GU} \\ &\Delta R_u^{GU} \le P_t^{GU} - P_{t-1}^{GU} \le \Delta R_d^{GU}, \end{aligned} \tag{1}$$

where η_{GU} is the gas–electricity conversion efficiency of the gas-fired unit; L_{CH_4} is the calorific value of methane, which is usually taken as 36 MJ/m^3; r is the conversion rate of the calorific value and power, which is usually taken as 3.6%; $P_{\max}^{GU}$ and $P_{\min}^{GU}$ are the upper and lower limits of the gas-fired unit, respectively; and ΔR_d^{GU} and ΔR_u^{GU} are the upper and lower limits of climbing constraints in the gas-fired unit, respectively.

The heating power of the oxygen-rich combustion capture unit is the heating power of the gas-fired unit, and the electricity-generating power and heat-producing power of the back-pressure

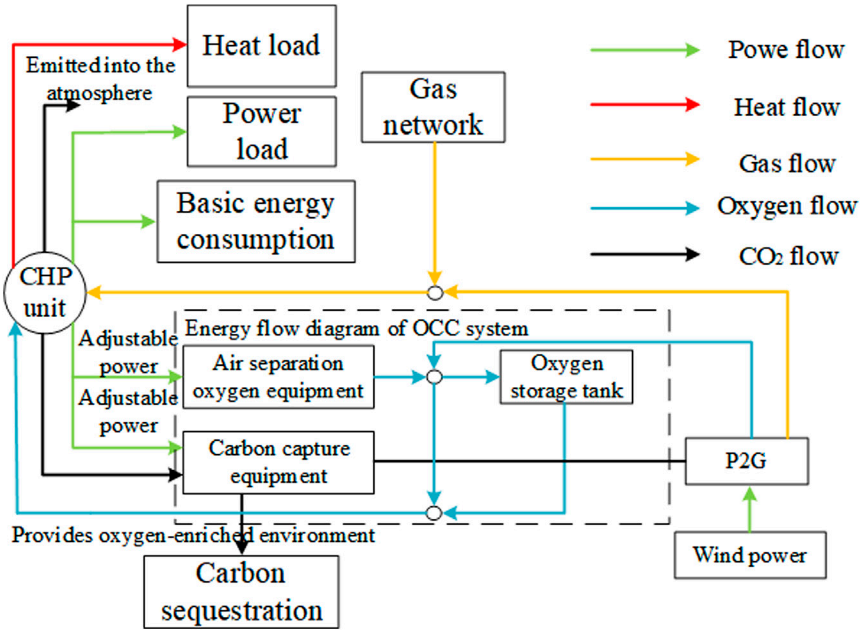

FIGURE 2
Energy flow diagram for oxygen-rich combustion capture units.

unit present a linear mathematical relationship in an approximate manner, with the specific expression as follows:

$$E_t^{OCC} = A_{GU} P_t^{GU}, \tag{2}$$

where E_t^{OCC} is the heat-producing power of the oxygen-rich combustion capture unit at time t and A_{GU} is the heat-to-power ratio of the gas-fired unit.

The introduction of the oxygen-rich combustion capture system will change the structure of the gas-fired unit to cause part of the energy loss, known as the baseline energy consumption P_B^{OCC}, which does not change with the change in the operating status of the unit and can be considered a fixed value. In addition, the unit needs to consume part of the electrical energy to maintain the operation of the oxygen-rich combustion capture system, and its operational energy consumption mainly includes the air separation oxygen generation equipment and carbon capture equipment; then, the energy consumption of the oxygen-rich combustion capture system P_t^{OCC} is shown as follows:

$$\begin{cases} P_t^{\mathrm{OCC}} = P_t^{\mathrm{CCE}} + P_t^{\mathrm{ASO}} \\ P_t^{\mathrm{CCE}} = \lambda_{\mathrm{CCE}} m_t^{\mathrm{CCE}} = \lambda_{\mathrm{CCE}} \beta_t^{\mathrm{CCE}} e_{\mathrm{G}} P_t^{\mathrm{GU}} \\ P_t^{\mathrm{ASO}} = \lambda_{\mathrm{ASO}} O_t^{\mathrm{ASO}} \end{cases}$$
$$O_t^{\mathrm{OCC}} = \alpha_{\mathrm{OCC}} P_t^{\mathrm{GU}} \tag{3}$$

where $t = 1, 2, 3..., T$ is the operational phase, the value of which is taken as 24; P_t^{CCE} and P_t^{ASO} are the power consumption of the carbon capture equipment and the air separation oxygen generation equipment at time t, respectively; m_t^{CCE} is the CO_2 capture mass of the carbon capture equipment at time t; λ_{CCE} and λ_{ASO} are the unit operating energy consumption of the carbon capture equipment and the air separation oxygen generation equipment, respectively; β_t^{CCE} and e_{G} are the carbon capture level of the carbon capture equipment and the carbon emission intensity of the gas turbine at time t, respectively; and O_t^{ASO} is the amount of oxygen produced by the air separation oxygen generation equipment at time t.

The oxygen consumption O_t^{OCC} in the oxygen-rich combustion capture unit t is shown as follows:

$$O_t^{\mathrm{OCC}} = \alpha_{\mathrm{OCC}} P_t^{\mathrm{GU}}, \tag{4}$$

where α_{OCC} is the oxygen consumption per unit of the output power when the oxygen-rich combustion capture unit is in operation.

Zhang et al. (2022) proved the process flow and equipment operation steps of traditional air technology to be basically the same as those of oxygen-rich combustion capture technology. Technically, the two operation modes can be converted to each other, and the switching time is usually less than 1/3 h. Thus, the influence of different modes of conversion is ignored. The restart time of the air separation oxygen generation equipment is longer with larger start-up energy consumption and minimum operating power. Therefore, the carbon capture equipment will stop running in the air operation mode, the unit exits the oxygen-rich combustion operation state, and the oxygen produced by the air separation oxygen generation equipment is stored in the oxygen tank. Then, the oxygen-rich combustion capture system collectively consumes energy as follows:

$$\begin{cases} P_t^{\mathrm{CCE}} = 0 \\ P_t^{\mathrm{ASO}} \geq a_{\min}^{ASO} P_{\max}^{ASO} \\ O_t^{\mathrm{OCC}} = 0, \end{cases} \tag{5}$$

where $a_{\min}^{ASO}$ and $P_{\max}^{ASO}$ are the minimum operating coefficient and the upper limit of the electrical power consumption of the air separation oxygen generation equipment, respectively.

10.3389/fenrg.2024.1296709

The net output power of the oxygen-rich combustion capture unit $P^{OCC}_{t,N}$ represents the overall external power generation of the unit. The net output power at time period t is shown as follows:

$$P^{\mathrm{OCC}}_{t,\mathrm{N}} = \left(1 - \lambda_{\mathrm{CCE}}\beta^{\mathrm{CCE}}_{t} e_{\mathrm{G}}\right)P^{\mathrm{GU}}_{t} - P^{\mathrm{OCC}}_{\mathrm{B}} - P^{\mathrm{ASO}}_{t}. \tag{6}$$

The CO_2 generated from the operation of the unit is mostly absorbed by the carbon capture equipment, and a small amount of it is emitted into the atmosphere. The net carbon emissions from the oxygen-rich combustion capture unit at time t are shown as follows:

$$m^{\mathrm{OCC}}_{t} = \left(1 - \beta^{\mathrm{CCE}}_{t}\right)e_{\mathrm{G}}P^{\mathrm{GU}}_{t}. \tag{7}$$

Zhu et al. (2022) defined the correlation between the net external power generation output and the net carbon emissions of a carbon capture unit as the "electro–carbon characteristic" of the unit, which is expressed as follows for an oxygen-rich combustion capture unit:

$$\begin{aligned} m^{\mathrm{OCC}}_{t} &= \frac{\left(1 - \beta^{\mathrm{CCE}}_{t}\right)e_{\mathrm{G}}}{1 - \lambda_{\mathrm{CCE}}\beta^{\mathrm{CCE}}_{t}e_{\mathrm{G}}}\left(P^{\mathrm{OCC}}_{t,\mathrm{N}} + P^{\mathrm{OCC}}_{t,\mathrm{B}} + P^{\mathrm{ASO}}_{t}\right), \\ 0 &\le \beta^{\mathrm{CCE}}_{t} \le \beta^{\max}_{\mathrm{CCE}} \end{aligned} \tag{8}$$

where $\beta^{\max}_{\mathrm{CCE}}$ is the limiting capture level of the carbon capture equipment.

When the oxygen-rich combustion capture unit is in operation, the CO_2 captured by the carbon capture equipment can be used either as a reaction feedstock for the power-to-gas equipment or for carbon sequestration, which can be expressed as follows:

$$m^{\mathrm{CCE}}_{t} = \beta^{\mathrm{CCE}}_{t}e_{\mathrm{G}}P^{\mathrm{GU}}_{t} = m^{\mathrm{CCE}}_{t,\mathrm{P2G}} + m^{\mathrm{CCE}}_{t,\mathrm{CS}}, \tag{9}$$

where $m^{\mathrm{CCE}}_{t,\mathrm{P2G}}$ is the mass supplied by the carbon capture equipment to the power-to-gas equipment at time t and $m^{\mathrm{CCE}}_{t,\mathrm{CS}}$ is the carbon mass sequestered at time t.

Based on the above analysis, the upper and lower limits of the net output power of the oxygen-rich combustion capture unit are introduced as follows:

$$\begin{cases} P^{\mathrm{OCC}}_{\mathrm{N,min}} \le P^{\mathrm{OCC}}_{t,\mathrm{N}} \le P^{\mathrm{OCC}}_{\mathrm{N,max}} \\ P^{\mathrm{OCC}}_{\mathrm{N,max}} = P_{\max}{}^{\mathrm{GU}} - P^{\mathrm{OCC}}_{t,\mathrm{B}} - a_{\min}{}^{\mathrm{ASO}}P_{\max}{}^{\mathrm{ASO}} \\ P^{\mathrm{OCC}}_{\mathrm{N,min}} = (1 - \lambda_{\mathrm{CCE}}\beta^{\max}_{\mathrm{CCE}}\, e_{\mathrm{G}})P_{\min}{}^{\mathrm{GU}} - P^{\mathrm{OCC}}_{t,\mathrm{B}} - P_{\max}{}^{\mathrm{ASO}} \end{cases} \tag{10}$$

In addition, the following power constraints need to be met when operating the air separation oxygen generation equipment:

$$a^{ASO}_{\min}P^{ASO}_{\max} \le P^{PSO}_{t} \le P^{ASO}_{\max}. \tag{11}$$

Oxygen storage tanks can achieve the use of oxygen across different time periods and store the oxygen in the form of liquid. Regarding the storage or discharge period, the form of oxygen is usually gaseous. In addition, the model for oxygen storage tanks in the gaseous form is presented as follows:

$$\begin{cases} O^{OT}_{\min} \le O^{\mathrm{OT}}_{t} \le O^{OT}_{\max} \\ 0 \le O^{\mathrm{OT}}_{t,\mathrm{out}} \le O^{\mathrm{OT}}_{\max,\mathrm{out}} \\ 0 \le O^{\mathrm{OT}}_{t,\mathrm{in}} \le O^{\mathrm{OT}}_{\max,\mathrm{in}} \\ O^{\mathrm{OT}}_{t} = (1 - \alpha_{\mathrm{OT}})O^{\mathrm{OT}}_{t-1} + \eta^{\mathrm{OT}}_{\mathrm{in}}O^{\mathrm{OT}}_{t,\mathrm{in}} - \dfrac{O^{\mathrm{OT}}_{t,\mathrm{out}}}{\eta^{\mathrm{OT}}_{\mathrm{out}}} \\ O^{\mathrm{OT}}_{t,\mathrm{in}}O^{\mathrm{OT}}_{t,\mathrm{out}} = 0 \\ O^{\mathrm{OT}}_{1} = O^{\mathrm{OT}}_{24}, \end{cases} \tag{12}$$

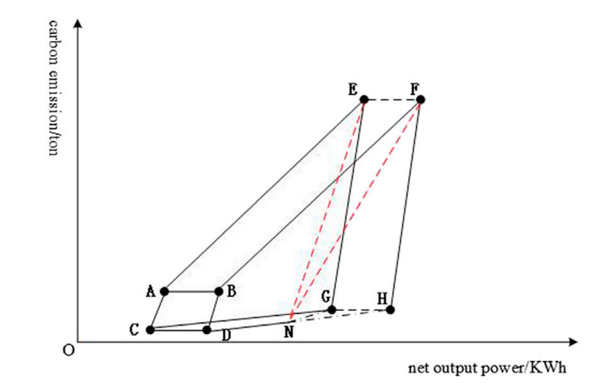

FIGURE 3
Electric carbon characteristics of oxygen-rich combustion capture units.

where $O^{OT}_{\max}$ and $O^{OT}_{\min}$ are the upper and lower limits of the oxygen storage tank capacity, respectively; $O^{\mathrm{OT}}_{t,\mathrm{out}}$ and $O^{\mathrm{OT}}_{\max,\mathrm{out}}$ are the oxygen release capacity and maximum oxygen release capacity at time t, respectively; $O^{\mathrm{OT}}_{t,\mathrm{in}}$ and $O^{\mathrm{OT}}_{\max,\mathrm{in}}$ are the oxygen storage capacity and the maximum oxygen storage capacity at time t, respectively; α_{OT} is the dissipation factor of the oxygen storage tank; $\eta^{\mathrm{OT}}_{\mathrm{in}}$ and $\eta^{\mathrm{OT}}_{\mathrm{out}}$ are the oxygen storage and discharge efficiencies, respectively; and O^{OT}_{24} and O^{OT}_{1} indicate the amount of oxygen stored in the tanks at the beginning and end of the scheduling period, respectively.

Point A: $P^{\mathrm{ASO}} = P^{ASO}_{\max}, P^{\mathrm{GU}} = P^{GU}_{\min}, P^{\mathrm{CCE}} = 0$
Point B: $P^{\mathrm{ASO}} = a^{ASO}_{\min}P^{ASO}_{\max}, P^{\mathrm{GU}} = P^{GU}_{\min}, P^{\mathrm{CCE}} = 0$
Point C: $P^{\mathrm{ASO}} = P^{ASO}_{\max}, P^{\mathrm{GU}} = P^{GU}_{\min}, P^{\mathrm{CCE}} = \lambda_{\mathrm{CCE}}\beta^{CCE}_{\max}e_{\mathrm{G}}P^{GU}_{\min}$
Point D: $P^{\mathrm{ASO}} = a^{ASO}_{\min}P^{ASO}_{\max}, P^{\mathrm{GU}} = P^{GU}_{\min}, P^{\mathrm{CCE}} = \lambda_{\mathrm{CCE}}\beta^{CCE}_{\max}e_{\mathrm{G}}P^{GU}_{\min}$
Point E: $P^{\mathrm{ASO}} = P^{ASO}_{\max}, P^{\mathrm{GU}} = P^{GU}_{\max}, P^{\mathrm{CCE}} = 0$
Point F: $P^{\mathrm{ASO}} = a^{ASO}_{\min}P^{ASO}_{\max}, P^{\mathrm{GU}} = P^{GU}_{\max}, P^{\mathrm{CCE}} = 0$
Point G: $P^{\mathrm{ASO}} = P^{\mathrm{ASO}}_{\max}, P^{\mathrm{GU}} = P^{\mathrm{GU}}_{\max}, P^{\mathrm{CCE}} = \lambda_{\mathrm{CCE}}\beta^{\mathrm{CCE}}_{\max}e_{\mathrm{G}}P^{\mathrm{GU}}_{\min}$
Point H: $P^{\mathrm{ASO}} = a^{ASO}_{\min}P^{ASO}_{\max}, P^{\mathrm{GU}} = P^{GU}_{\max}, P^{\mathrm{CCE}} = \lambda_{\mathrm{CCE}}\beta^{CCE}_{\max}e_{\mathrm{G}}P^{GU}_{\min}$

In Figure 3, assuming that the amount of oxygen produced by the air separation oxygen generation equipment at point N exactly meets the demand for oxygen-rich operation, when approaching from point N to point H, the carbon emission increases, the air separation oxygen generation equipment that maintains the minimum power cannot meet the demand for oxygen-rich unit operation, and the difference in oxygen can be supplied by the oxygen storage tank. Therefore, ABCDNGE is the oxygen-rich operation area of the unit when using the oxygen storage tank. At this time, the phenomena of discarding oxygen occur. Pentahedron NHGEF presents the extra oxygen-rich operation area in the unit equipped with the oxygen storage tank, which indicates that when the net output of the oxygen-rich combustion capture unit is larger, the energy consumption of the air separation oxygen equipment is reduced, and the oxygen storage tank can be used to supplement for the difference in oxygen. When the net output of the unit is smaller, the energy consumption of the air oxygen equipment can be improved to add oxygen into the oxygen storage tank. The analysis shows that the oxygen-rich combustion capture unit equipped with the oxygen storage tank can expand the scope of operation.

Therefore, the operation and maintenance (O&M) cost of the oxygen-rich combustion capture unit is shown as follows:

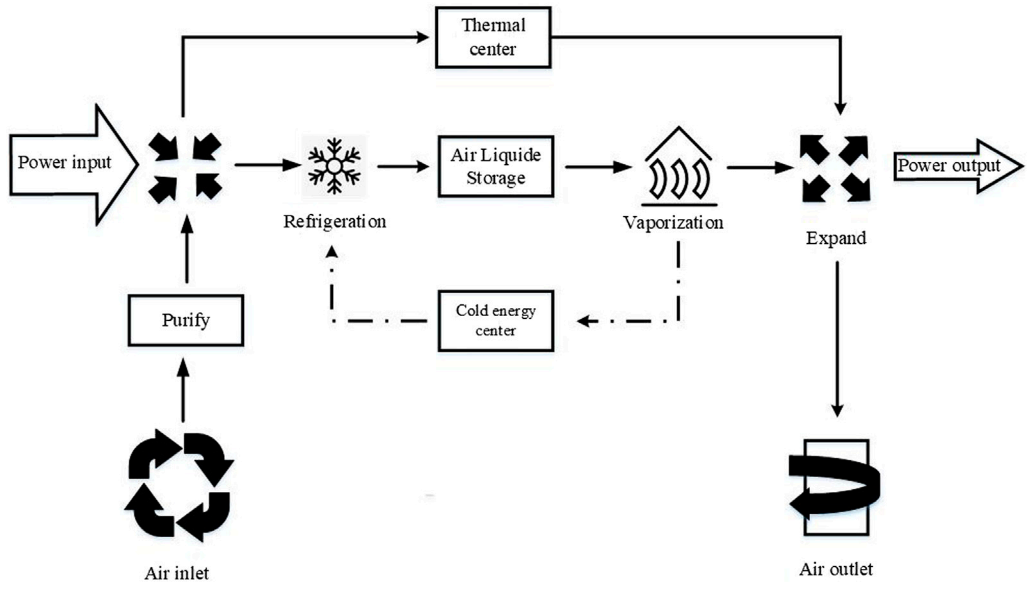

FIGURE 4
Air liquid energy storage architecture.

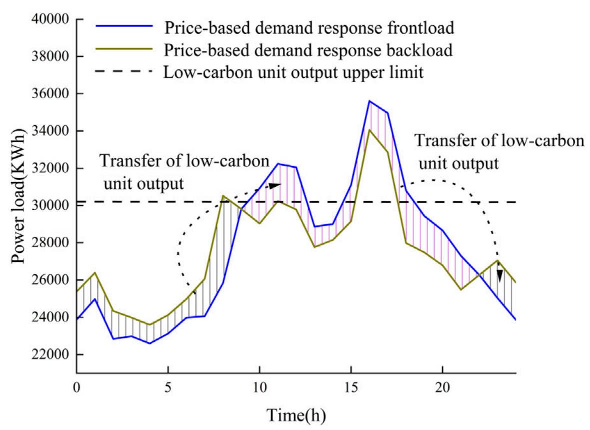

FIGURE 5
Demand response low-carbon principles.

$$S^{\mathrm{OCC}}_{t,\mathrm{yw}} = s^{\mathrm{ASO}}_{\mathrm{yw}} P^{\mathrm{ASO}}_{t} + s^{\mathrm{CCE}}_{\mathrm{yw}} P^{\mathrm{CCE}}_{t} + s^{\mathrm{GU}}_{\mathrm{yw}} P^{\mathrm{GU}}_{t} + s^{\mathrm{OT}}_{\mathrm{yw}} \left(O^{\mathrm{OT}}_{t,\mathrm{in}} + O^{\mathrm{OT}}_{t,\mathrm{out}} \right), \quad (13)$$

where $s^{\mathrm{ASO}}_{\mathrm{yw}}$、$s^{\mathrm{CCE}}_{\mathrm{yw}}$、$s^{\mathrm{GU}}_{\mathrm{yw}}$、$s^{\mathrm{OT}}_{\mathrm{yw}}$ are the O&M cost factors for the air separation oxygen generation equipment, carbon capture equipment, gas-fired units, and oxygen storage tanks, respectively.

Detailed modeling of the internal equipment in the IES can be found in Supplementary Material. Air liquid energy storage architecture is shown in Figure 4.

3 Low-carbon strategies based on low-carbon demand response

DR resources mainly include price-based demand response (PDR) and incentive-based demand response (IDR). PDR guides users to engage in reasonable electricity consumption behavior by changing electricity prices, thereby adjusting electricity consumption plans. IDR includes interruptible loads, demand-side bidding, emergency demand-side response, and direct load control. The power department usually first signs a contract with the load agency (aggregator) to classify and integrate various users who can improve DR resources, and finally, it is uniformly regulated by the dispatch center (Tian et al., 2023).

DR resources can optimize the output plans of units with different carbon emission intensities by changing the load curve (Zhang et al., 2021), thereby achieving the effect of reducing system carbon emissions. The low-carbon principle of price-based demand response is shown in Figure 5.

As shown in Figure 5, the demand response can shift some load from the peak period to the valley period. During the peak period, when the net output of low-carbon units has reached the upper limit, the output of high-cost and high-carbon emission thermal power units supplies the difference in the load. After the price-based demand response, this part of the load is supplied by the output of low-cost, low-carbon emission carbon capture units during the valley period, or additional consumption of low-marginal cost, carbon-neutral wind power generation, which effectively reduces the carbon emissions of the system.

3.1 Price-based demand response models

The electricity load demand response model in this article adopts the price demand response elasticity matrix method. The electricity load change rate and electricity price change rate can be characterized by the elasticity index of electricity consumption and electricity price, and its expression is as follows:

$$m = \frac{\Delta L}{L}\left(\frac{\Delta c_p}{c_p}\right)^{-1}, \tag{25}$$

where m is the elasticity index of electricity consumption and electricity price; c_p and Δc_p are the differences in the electricity price in the peak-valley period and the fixed electricity price; and L and ΔL are the amount of electricity consumption and load response before the load response, respectively.

Based on the ratio of the time-of-use electricity price to the fixed electricity price, the following elasticity matrix is established:

$$N_e = \begin{bmatrix} N_{11} & N_{12} & \cdots & N_{1m} \\ N_{21} & N_{22} & \cdots & N_{2\mathrm{m}} \\ \vdots & \vdots & \ddots & \vdots \\ N_{n1} & N_{\mathrm{n}2} & \cdots & N_{nm} \end{bmatrix}, \tag{26}$$

$$N_{ii} = \frac{\Delta L_i}{L_i}\left(\frac{\Delta c_{pi}}{c_{pi}}\right)^{-1}, \tag{27}$$

$$N_{ij} = \frac{\Delta L_i}{L_i}\left(\frac{\Delta c_{pj}}{c_{pj}}\right)^{-1}, \tag{28}$$

where N_{ii} is the self-elasticity coefficient; N_e is the elasticity matrix of electricity consumption and electricity price; L_i and ΔL_i are the amount of electricity and its variation for the user in time period i, respectively; N_{ij} is the cross-elasticity coefficient; and c_{pi} and Δc_{pi} and c_{pj} and Δc_{pj} are the electricity price and its variation in time periods i and j, respectively.

Based on the electricity elasticity matrix M_e, the customer load response is obtained as follows:

$$\Delta L_e(t) = \begin{Bmatrix} L_{e,0,f} & 0 & 0 \\ 0 & L_{e,0,p} & 0 \\ 0 & 0 & L_{e,0,g} \end{Bmatrix} \cdot N_e \begin{Bmatrix} \dfrac{\Delta c_{e,pf}}{c_{e,p0,f}} \\ \dfrac{\Delta c_{e,pp}}{c_{e,p0,p}} \\ \dfrac{\Delta c_{e,pg}}{c_{e,p0,g}} \end{Bmatrix}, \tag{29}$$

where $L_{e,0,f}$, $L_{e,0,p}$, and $L_{e,0,g}$ denote the electricity consumption in the peak, valley, and flat periods before the price-based incentive, respectively; $\Delta L_e(t)$ is the amount of electricity use transferred after the price-based incentive; and $c_{e,p0,f}$, $c_{e,p0,p}$, and $c_{e,p0,g}$ and $\Delta c_{e,pf}$, $\Delta c_{e,pp}$, and $\Delta c_{e,pg}$ denote the difference between the fixed electricity price and time-of-use electricity price, respectively.

Since gas energy has the same commodity property as electricity, the gas load can be adjusted based on the published time-of-day gas price, so the IDR model of the gas load can also be modeled by the method of the price-type elasticity matrix. Analogous to the electricity price-based IDR model, the relationship between the gas load and the time-of-day gas price also exists, as shown in Eq. (29), which is expressed as follows:

$$\Delta L_g(t) = \begin{Bmatrix} L_{g,0,f} & 0 & 0 \\ 0 & L_{g,0,p} & 0 \\ 0 & 0 & L_{g,0,g} \end{Bmatrix} \cdot N_g \begin{Bmatrix} \dfrac{\Delta c_{g,pf}}{c_{g,p0,f}} \\ \dfrac{\Delta c_{g,pp}}{c_{g,p0,p}} \\ \dfrac{\Delta c_{g,pg}}{c_{g,p0,g}} \end{Bmatrix}, \tag{30}$$

where $\Delta L_g(t)$ is the amount of the gas load shifted after the price-based incentive for the gas; $L_{g,0,f}$, $L_{g,0,p}$, and $L_{g,0,g}$ denote the amount of gas used in the peak, valley, and flat periods before the price-based incentive, respectively; $c_{g,p0,f}$, $c_{g,p0,p}$, and $c_{g,p0,g}$ and $\Delta c_{g,pf}$, $\Delta c_{g,pp}$, and $\Delta c_{g,pg}$ represent the difference between fixed and time-of-day gas prices, respectively; and N_g denotes the elasticity matrix of gas price and gas consumption.

3.2 Incentive-based demand response

Incentive-based demand response refers to the direct reduction or interruption of a portion of the load by users based on compensation and incentive mechanisms established by energy operators during the peak period of load or in emergency situations. The incentive demand response constructed in this article includes electricity load, gas load, heat load, and cooling load.

3.2.1 Incentive-based electricity load and gas load

When the system is in peak operation, the electricity/gas consumer has a prior agreement with the energy operator to curtail part of the load, and its mathematical model is shown as follows:

$$E_{\mathrm{IDR,e}}(t) = \varepsilon_{\mathrm{e}} c_e(t) L_{\mathrm{e,cut}}(t), \tag{31}$$

$$E_{\mathrm{IDR,g}}(t) = \varepsilon_g c_g(t) L_{\mathrm{g,cut}}(t), \tag{32}$$

where ε_{e} and ε_g are reduction allowance factors for electricity and gas loads, respectively; $L_{\mathrm{e,cut}}(t)$ and $L_{\mathrm{g,cut}}(t)$ are the amount of electricity and gas loads curtailed by the user, respectively; and $E_{\mathrm{IDR,e}}(t)$ and $E_{\mathrm{IDR,g}}(t)$ are the costs of incentive subsidies for users to curtail their electricity and gas loads, respectively.

For the reduction in electricity and gas loads, in order to prevent too much impact on the life of users, the amount of adjustment of electricity and gas loads at moment t should be within a certain range, and the total load change within 1 day should also meet the limit as follows:

$$\begin{cases} L_{\mathrm{e,cut}}(t) \le \varphi_{\mathrm{e,cut}} L_{\mathrm{e,0}}(t) \\ \sum_{t=1}^{T} L_{\mathrm{e,cut}}(t) \le \varphi_{\mathrm{total}}^{e} \sum_{t=1}^{T} L_{\mathrm{e,0}}(t) \end{cases}, \tag{33}$$

$$\begin{cases} L_{\mathrm{g,cut}}(t) \le \varphi_{\mathrm{g,cut}} L_{\mathrm{g,0}}(t) \\ \sum_{t=1}^{T} L_{\mathrm{g,cut}}(t) \le \varphi_{\mathrm{total}}^{g} \sum_{t=1}^{T} L_{\mathrm{g,0}}(t) \end{cases}, \tag{34}$$

where $L_{\mathrm{e,0}}(t)$ and $L_{\mathrm{g,0}}(t)$ are the initial electricity load and initial gas load, respectively; $\varphi_{\mathrm{e,cut}}$ and $\varphi_{\mathrm{g,cut}}$ are the upper limits of the reduction rates for electricity and gas loads, respectively; and $\varphi_{\mathrm{total}}^{e}$ and $\varphi_{\mathrm{total}}^{\mathrm{g}}$ are the upper limits of the total reduction rates for electricity and gas loads, respectively.

3.2.2 Modeling of heat/cooling load

Considering the time delay and perceptual ambiguity of heat and cooling loads, adjusting the temperature within the comfort range will not have a significant impact on users. The quantitative relationship between the heat/cooling load demand and indoor and outdoor temperatures is shown as follows:

$$\begin{cases} L_h(t) = f(T_{h,in}(t)) = 3.6\left[S\varepsilon(T_{h,in}(t) - T_{h,out}(t)) + \frac{CS}{\Delta t}(T_{h,in}(t) - T_{h,in}(t-1))\right] \\ L_c(t) = f(T_{c,in}(t)) = 3.6\left[S\varepsilon(T_{c,in}(t) - T_{c,out}(t)) + \frac{CS}{\Delta t}(T_{c,in}(t) - T_{c,in}(t-1))\right], \end{cases} \tag{35}$$

where ε is the indoor heat loss per unit of the floor area under the condition of a difference in temperature; S is the indoor area of a building; C is the specific heat capacity per unit of the floor area; $T_{h,in}(t)$ and $T_{h,out}(t)$ are the indoor and outdoor temperatures of the heating system, respectively; and $T_{c,in}(t)$ and $T_{c,out}(t)$ are the indoor and outdoor temperatures of the cooling system, respectively.

The mathematical model of the demand response for the heat load and cooling load can be expressed as follows:

$$\begin{cases} \Delta L_h(t) = f(T_{h,in}(t)) - f(T_{h,in}(t) - \Delta T_{h,in}(t)), 0 \le \Delta L_h(t) \le \Delta L_{h,max} \\ T^{min} \le T_{h,in}(t) - \Delta T_{h,in}(t) \le T^{max} \end{cases}, \tag{36}$$

$$\begin{cases} \Delta L_c(t) = f(T_{c,in}(t)) - f(T_{c,in}(t) - \Delta T_{c,in}(t)), 0 \le \Delta L_c(t) \le \Delta L_{c,max} \\ T^{min} \le T_{c,in}(t) - \Delta T_{c,in}(t) \le T^{max} \end{cases}, \tag{37}$$

where $\Delta T_{h,in}(t)$ and $\Delta T_{c,in}(t)$ are the outdoor temperature changes for heating and cooling systems, respectively; $\Delta L_h(t)$ and $\Delta L_c(t)$ are the changes in the heat and cooling loads of the user at time t, respectively; $\Delta L_{h,max}$ and $\Delta L_{c,max}$ are the upper limits of the amount of variation in the heat and cooling loads of the users, respectively; and T^{max} and T^{min} are the upper and lower temperature limits where the user is in the comfort range, respectively.

Due to the time delay and ambiguity of user requirements for indoor temperature comfort, the impact of small changes in the heat/cooling load on user comfort is relatively small. However, when the heat/cooling load changes significantly, the impact on user comfort is significant, so the impact of the heat/cooling load change on user comfort is not linearly correlated. Therefore, this article adopts a stepped compensation method to encourage users to change the heat/cooling load. The compensation cost for the user heat/cooling load at time t is shown as follows:

$$E_{h,IDR}(t) = \varepsilon_{h,IDR} \Delta L_h(t), \tag{38}$$

$$E_{c,IDR}(t) = \varepsilon_{c,IDR} \Delta L_c(t), \tag{39}$$

where $E_{h,IDR}(t)$ and $E_{c,IDR}(t)$ are the cost of incentive-based IDR subsidies for heat and cooling loads, respectively and $\varepsilon_{h,IDR}$ and $\varepsilon_{c,IDR}$ are the subsidy factors for changes in heat and cooling loads, respectively.

Taking the heat load incentive compensation as an example, the greater the deviation degree of heat load, the greater the impact on user comfort. This article adopts a stepped subsidy coefficient, which varies in a stepped manner based on the impact of the actual load on user comfort. The greater the deviation degree, the greater the subsidy coefficient, which can be expressed as follows:

$$\varepsilon_{h,IDR} = \begin{cases} \varepsilon_{h,IDR} & 0 < |\Delta L_h(t)| < \alpha_1 \\ (1 + \lambda_{h,IDR})\varepsilon_{h,IDR} & \alpha_1 \le |\Delta L_h(t)| \le \alpha_2 \\ (1 + 2\lambda_{h,IDR})\varepsilon_{h,IDR} & |\Delta L_h(t)| > \alpha_2, \end{cases} \tag{40}$$

where $\lambda_{h,IDR}$ is the penalty factor of the subsidy coefficient for the heat load changes and α_1 and α_2 are the dividing boundaries for the amount of the heat load change, respectively.

Similarly, the subsidy coefficients for changes in cooling loads can be expressed as follows:

$$\varepsilon_{c,IDR} = \begin{cases} \varepsilon_{c,IDR} & 0 < |\Delta L_c(t)| < \beta_1 \\ (1 + \lambda_{c,IDR})\varepsilon_{c,IDR} & \beta_1 \le |\Delta L_c(t)| \le \beta_2 \\ (1 + 2\lambda_{c,IDR})\varepsilon_{c,IDR} & |\Delta L_c(t)| > \beta_2, \end{cases} \tag{41}$$

where $\lambda_{c,IDR}$ is the penalty factor of the subsidy coefficient for the cooling load changes and β_1 and β_2 are the dividing boundaries for the amount of the cooling load change, respectively.

4 Stepped carbon trading models

At present, the domestic carbon emission trading market has started trial operation, guiding various industries to achieve low-carbon emissions through policies. The main methods of allocating carbon emission reduction quotas include free allocation, paid allocation, and mixed allocation. Currently, free allocation is mainly used in China. The stepped carbon trading mechanism mainly consists of three parts: initial carbon emission quotas, actual carbon emissions, and carbon trading costs (Guan et al., 2018; Chrispim, 2021; Liang et al., 2021).

4.1 Modeling of carbon emission quotas

The main source of carbon emissions in the system consists of two components, namely, the oxygen-rich combustion unit and the equivalent emissions from power purchases. The model of carbon emission quotas is shown as follows:

$$\begin{aligned} G_{t,pe}^{IES} &= G_{t,pe}^{buy} + G_{t,pe}^{OCC} \\ G_{t,pe}^{buy} &= g_p P_t^{buy} \\ G_{t,pe}^{OCC} &= g_h (g_{p-h} P_t^{GU} + 3.6 E_t^{GU}), \end{aligned} \tag{42}$$

where $G_{t,pe}^{IES}$, $G_{t,pe}^{buy}$, and $G_{t,pe}^{OCC}$ are carbon emission quotas for the IES, purchased electricity, and oxygen-rich combustion units, respectively; g_p and g_h are the carbon emission intensity per unit of electrical and thermal power, respectively, which are usually taken as 0.728 kg CO_2/(KWh) and 0.102 kg CO_2/MJ; P_t^{buy} is the amount of purchased electricity of the system at time t; and g_{p-h} is the electric heat conversion factor, which is usually taken as 6 MJ CO_2/(KWh).

4.2 Modeling of actual carbon emissions

In this system, it is assumed that all purchased electricity comes from coal-fired units and that the P2G converter in the system will reduce some of the carbon emissions. Therefore, the model of the actual carbon emissions is shown as follows:

$$\begin{aligned} G_{t,\mathrm{pf}}^{\mathrm{IES}} &= G_{t,\mathrm{pf}}^{\mathrm{buy}} + m_t^{\mathrm{OCC}} - m_t^{\mathrm{P2G}} \\ G_{t,\mathrm{pf}}^{\mathrm{buy}} &= a_1\left(P_t^{\mathrm{buy}}\right)^2 + b_1 P_t^{\mathrm{buy}} + c_1, \end{aligned} \tag{43}$$

where $G_{t,\mathrm{pf}}^{\mathrm{IES}}$, $G_{t,\mathrm{pf}}^{\mathrm{buy}}$, and $G_{t,\mathrm{pf}}^{\mathrm{buy}}$ are the actual carbon emissions of the IES and purchased electricity, respectively; a_1、b_1、c_1 are the carbon emission factors for coal power; and a_2、b_2、c_2 are the carbon emission coefficients for natural gas energy supply.

4.3 Modeling of the stepped carbon transaction cost

In order to ensure a reasonable control system of carbon emissions, this paper adopts a stepped carbon transaction cost model. The stepped pricing mechanism divides multiple purchase intervals, and the more carbon emission rights to be purchased, the higher the purchase price of the corresponding interval. The stepped carbon transaction cost model can be expressed as follows:

$$F_{t,CO_2}^{IES} = \begin{cases} \lambda\left(G_{t,pf}^{IES} - G_{t,pe}^{IES}\right) \\ \lambda(1+\alpha)\left(G_{t,pf}^{IES} - G_{t,pe}^{IES} - l\right) + \lambda l \\ \lambda(1+2\alpha)\left(G_{t,pf}^{IES} - G_{t,pe}^{IES} - 2l\right) + \lambda(2+\alpha)l \\ \lambda(1+3\alpha)\left(G_{t,pf}^{IES} - G_{t,pe}^{IES} - 3l\right) + \lambda(3+3\alpha)l \\ \lambda(1+4\alpha)\left(G_{t,pf}^{IES} - G_{t,pe}^{IES} - 4l\right) + \lambda(4+6\alpha)l, \end{cases} \tag{44}$$

where F_{t,CO_2}^{IES} is the systematic carbon transaction cost at time t; λ is the carbon trading base price; l is the length of the carbon emission interval; and α is the growth rate of carbon trading prices.

5 Optimization model of the integrated energy system

5.1 Objective function

The model proposed in this article comprehensively considers the cost of purchasing natural gas from the system, the cost of purchasing electricity from the power grid, the cost of operation and maintenance, the cost of carbon storage, the cost of carbon trading, the cost of wind abandonment penalty, and the cost of load loss penalty, with the objective function of minimizing the total operating cost for optimization. The objective function is shown as follows:

$$\min f = \sum_{t=1}^{T}\left(F_{t,buy}^{IES} + F_{t,wh}^{IES} + F_{t,CO_2}^{IES} + F_{t,CS}^{CO_2} + F_{t,cf}^{FD} + F_{t,fh}^{IES} + F_{t,IDR}^{IES}\right), \tag{45}$$

where $F_{t,buy}^{IES}$ is the cost of purchasing energy for the system at time t; $F_{t,wh}^{IES}$ is the cost of operating and maintaining the system at time t; $F_{t,CS}^{CO_2}$ is the cost of carbon sequestration at time t; and $F_{t,cf}^{FD}$ and $F_{t,fh}^{IES}$ are the system wind abandonment penalty cost and the electric load loss penalty cost at time t, respectively.

5.1.1 Cost of the purchased electricity

The system purchased energy cost includes two components: the purchased electricity cost and purchased gas cost. In addition, the price of the purchased electricity is decided by using the time-of-day electricity price mechanism:

$$F_{t,buy}^{IES} = s_t^{\mathrm{buy}} P_t^{\mathrm{buy}} + s_{t,gas}^{\mathrm{buy}} V_t^{\mathrm{buy}}, \tag{46}$$

where s_t^{buy} is the price at which the system purchases electricity from the grid at time t and $s_{t,gas}^{\mathrm{buy}}$ and V_t^{buy} are the price and volume of gas purchased by the system at time t, respectively.

5.1.2 Cost of operation and maintenance

$$\begin{aligned} F_{t,wh}^{IES} = {} & S_{t,yw}^{\mathrm{OCC}} + s_{yw}^{P2G} P_t^{P2G} + s_{yw}^{WT} P_t^{WT} + s_{yw}^{LAE} P_t^{LAE} + s_{yw}^{XHL} E_t^{XHL} \\ & + s_{yw}^{Kongtiao} P_t^{Kongtiao}, \end{aligned} \tag{47}$$

where s_{yw}^{P2G}, s_{yw}^{WT}, s_{yw}^{LAE}, s_{yw}^{XHL}, and $s_{yw}^{Kongtiao}$ are the O&M costs for the P2G equipment, wind power, liquefied natural gas (LNG) tanks, lithium bromide absorption refrigerant, and electric refrigeration and air conditioning, respectively.

5.1.3 Cost of carbon sequestration

Carbon sequestration costs are required to sequester the remaining CO_2 when the P2G equipment is unable to consume the captured CO_2, and the cost of carbon sequestration can be expressed as follows:

$$F_{t,CS}^{CO_2} = s_{CS}^{CO_2} m_{t,CS}^{CCE}, \tag{48}$$

where $s_{CS}^{CO_2}$ is the cost coefficient of carbon sequestration.

5.1.4 Cost of wind abandonment penalty and load loss penalty

In order to make the system realize the full consumption of new energy and reduce the occurrence of the wind abandonment phenomenon, the wind abandonment penalty cost is used to improve the wind power consumption rate of the system. The cost of the wind abandonment penalty is shown as follows:

$$F_{t,\mathrm{cf}}^{\mathrm{WP}} = s_{\mathrm{cf}}^{\mathrm{WP}}\left(P_t^{\mathrm{yc}} - P_t^{\mathrm{WP}}\right), \tag{49}$$

$$F_{t,fh}^{\mathrm{WP}} = s_{\mathrm{fh}}^{\mathrm{WP}}\left(P_t^{\mathrm{yc,Eload}} - P_t^{Load}\right), \tag{50}$$

where $s_{\mathrm{cf}}^{\mathrm{WP}}$ is the unit cost of wind abandonment penalties; P_t^{yc} and P_t^{WP} denote the predicted wind power output and wind power consumption power at time t, respectively; $s_{\mathrm{fh}}^{\mathrm{WP}}$ is the unit cost of load loss penalties; and $P_t^{\mathrm{yc,Eload}}$ and P_t^{Load} denote the predicted power of the load and the actual electrical load at time t, respectively.

5.1.5 Cost of the demand response

$$F_{\mathrm{IDR}} = \sum_{t=1}^{T}\left(E_{\mathrm{e,IDR}}(t) + E_{\mathrm{h,IDR}}(t) + E_{\mathrm{c,IDR}}(t) + E_{\mathrm{g,IDR}}(t)\right). \tag{51}$$

5.2 Constraints

5.2.1 System balance constraints

- Electrical power balance constraints

$$\begin{aligned} & P_{t,\mathrm{N}}^{\mathrm{OCC}} + P_t^{\mathrm{buy}} + P_t^{ELoadCur} + P_t^{LAE} + P_{t,\mathrm{load}}^{\mathrm{WP}} + P_t^{LNG} \\ & = P_t^{\mathrm{load}} + P_t^{Kongtiao} + P_t^{P2G} + P_t^{XHL}, \end{aligned} \tag{52}$$

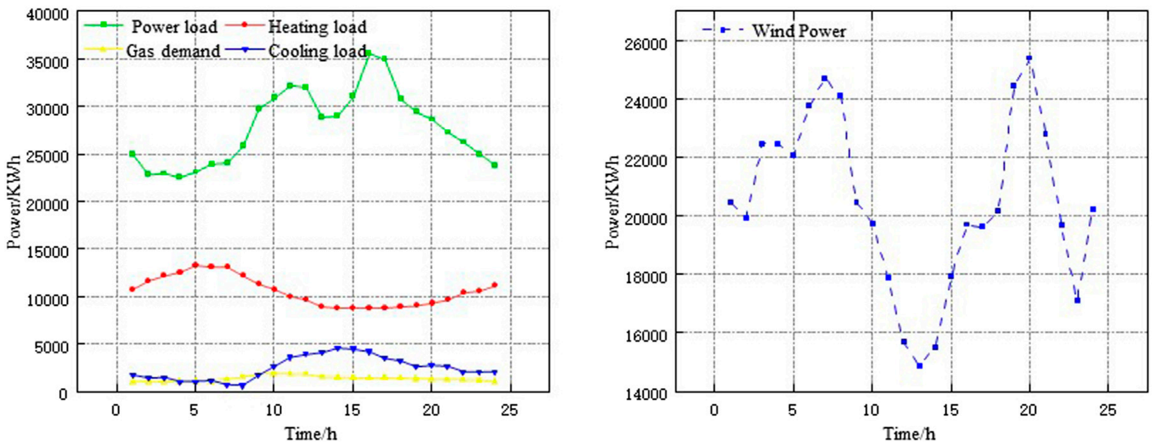

FIGURE 6
Comprehensive energy system load and wind power forecasts.

TABLE 1 Time-of-use electricity price and time-of-use gas price.

Initial electricity price	Time period	CNY/kWh/m^3
Valley	1:00–6:00, 23:00–24:00	0.5
Flat	7:00–8:00, 13:00–17:00	0.73
Peak	9:00–12:00, 18:00–22:00	1.21
Initial gas price	**Time period**	**CNY·m^{-3}**
Valley	23:00–24:00, 01:00–05:00	1.57
Flat	6:00–7:00, 13:00–16:00, 19:00–22:00	1.93
Peak	8:00–12:00, 17:00–18:00	2.16

where P_t^{LAE}, P_t^{LNG}, P_t^{XHL}, and $P_t^{EloadCur}$ are the discharge power of the energy storage system, the electrical energy released by the LNG gasification station in the gasification of natural gas, the power of electrical energy absorbed by the energy storage system, and the power of the system electrical load loss, respectively.

- Gas power balance constraints

$$V_t^{LNG} + V_t^{\mathrm{buy}} + V_t^{\mathrm{P2G}} = V_t^{\mathrm{GU}} + V_t^{load}, \tag{53}$$

where V_t^{LNG} and V_t^{load} are the natural gas power released from the LNG gasification station and the system natural gas load, respectively.

- Heat power balance constraint

$$E_t^{\mathrm{OCC}} + E_t^{\mathrm{P2G}} = E_t^{\mathrm{Load}} + E_t^{XHL}, \tag{54}$$

where E_t^{Load} is the heat load of the system and E_t^{XHL} is the heat power consumed by the residual heat of lithium bromide refrigeration.

- Cold power balance constraint

$$L_t^{LNG} + L_t^{LAE} + L_t^{kongtiao} + L_t^{XHL} = L_t^{Load}, \tag{55}$$

where L_t^{LNG}, L_t^{LAE}, $L_t^{kongtiao}$, L_t^{XHL}, and L_t^{Load} are the cold power released from the LNG gasification station, the cold power released from the energy storage unit, air-conditioning refrigeration, lithium bromide refrigeration, and the system cold load, respectively.

- Oxygen balance constraint

$$O_t^{\mathrm{ASO}} + O_t^{\mathrm{P2G}} + O_{t,\mathrm{out}}^{\mathrm{OT}} - O_{t,\mathrm{in}}^{\mathrm{OT}} - O_t^{\mathrm{loss}} = O_t^{\mathrm{OCC}}, \tag{56}$$

where O_t^{loss} is the amount of oxygen discarded at time t.

- Wind power operation constraint

$$0 \le P_t^{\mathrm{WP}} \le P_t^{\mathrm{yc}}. \tag{57}$$

5.2.2 LAES constraint

The liquid air energy storage (LAES) and discharge constraints and storage capacity constraints are shown as follows:

$$\begin{cases} 0 \le P_t^{cha} \le P_{\max}^{ch} U_t^{LAE,ch} \\ 0 \le P_t^{dis} \le P_{\max}^{dis} U_t^{LAE,dis} \\ U_t^{LAE,ch} U_t^{LAE,dis} \le 1 \\ U_t^{LAE,ch}, U_t^{LAE,dis} \in \{0,1\} \\ SOC_{\min}^{LAE} \le P_t^{LAE} \le SOC_{\max}^{LAE}, \end{cases} \tag{58}$$

TABLE 2 Basic parameters of the integrated energy system.

Parameter	Parameter symbol	Parameter value	Parameter unit
Liquid air energy storage (LAES) energy storage limit	$SOC_{\max}^{LAE}$	2,000	KW
LAES energy storage lower limit	$SOC_{\min}^{LAE}$	200	KW
Initial value of LAES energy storage for liquid air energy storage	P_0^{LAE}	200	KW
Refrigeration efficiency of lithium bromide waste heat refrigeration	η_L^{XHL}	0.7	
Volume ratio before and after gasification in the liquefied natural gas (LNG) gasification station	β_t^{LNG}	0.714	
Refrigeration efficiency during gasification of natural gas in the LNG gasification station	η_t^{LNG}	0.23	
Electricity production efficiency in the process of gasification of natural gas in the LNG gasification station	α_t^{LNG}	0.1	
Conversion efficiency of electric refrigeration	η_t^{EL}	3.1	
Unit operation and maintenance cost of the power-to-gas (P2G) equipment	s_{yw}^{P2G}	0.02	CNY/KWh
Wind power equipment unit operation and maintenance costs	s_{yw}^{WT}	0.02	CNY/KWh
Unit operation and maintenance cost of the liquefied natural gas tank	s_{yw}^{LAE}	0.02	CNY/KWh
Unit operation and maintenance cost of lithium bromide absorption refrigeration	s_{yw}^{XHL}	0.02	CNY/KWh
Operation and maintenance costs of electric refrigeration and air conditioning units	$s_{yw}^{Kongtiao}$	0.02	CNY/KWh
Unit curtailment penalty cost	$s_{\mathrm{cf}}^{\mathrm{WP}}$	0.6	CNY/KWh
Unit loss penalty cost	$s_{\mathrm{fh}}^{\mathrm{WP}}$	10	CNY/KWh
Gas unit climbing constraint upper limit	ΔR_d^{GU}	3,000	KW
Lower limit of the gas unit climbing constraint	ΔR_u^{GU}	0	KW
Oxygen tank capacity upper limit	$O_{\max}^{OT}$	10,000	m^3
Oxygen tank capacity lower limit	$O_{\min}^{OT}$	1,000	m^3
Maximum oxygen release capacity of the oxygen storage tank	$O_{\max,\mathrm{out}}^{\mathrm{OT}}$	2,500	m^3
Maximum oxygen storage capacity of the oxygen storage tank	$O_{\max,\mathrm{in}}^{\mathrm{OT}}$	2,500	m^3
Dissipation coefficient of the oxygen storage tank	α_{OT}	0.02	
Oxygen storage and oxygen release efficiency	$\eta_{\mathrm{in}}^{\mathrm{OT}}/\ \eta_{\mathrm{out}}^{\mathrm{OT}}$	0.95	
Oxygen storage tank scheduling initial period and end period	$O_{24}^{\mathrm{OT}}/O_1^{\mathrm{OT}}$	2,500	
Carbon trading base price	λ	200	CNY
Carbon emission interval length	l	2	Ton
Carbon trading price growth rate	α	0.25	

where $P_{\max}^{cha}$ and $P_{\max}^{dis}$ indicate the upper limits of storage and discharge power of LAES, respectively; $U_t^{LAE,cha}$ and $U_t^{LAE,dis}$ are the operating status of LAES at time *t*, respectively; and $SOC_{\max}^{LAE}$ and $SOC_{\min}^{LAE}$ indicate the upper and lower limits of the LAES.

5.2.3 System electrical load loss constraint

$$\begin{gathered} 0 \le P_t^{load} \le P_t^{\mathrm{load,yc}} \\ P_t^{EloadCur} + P_t^{load} = P_t^{\mathrm{load,yc}} \end{gathered} . \tag{59}$$

This article constructs a complete low-carbon economic optimization model for the IES, taking into account the system energy purchase cost, operation and maintenance cost, carbon trading cost, carbon sequestration cost, demand response cost, wind abandonment penalty, and load loss penalty. The optimal output plan for each unit and equipment with the minimum sum of multiple costs during the scheduling cycle can be obtained, resulting in the lowest total operating cost of the system.

TABLE 3 Basic parameters of oxygen-rich combustion capture technology.

Parameter	Parameter symbol	Parameter value	Parameter unit
Carbon capture equipment operation and maintenance costs	λ_{CCE}	0.0893	KW
Operation and maintenance costs of the air oxygen generator	λ_{ASO}	0.4	KW
Oxygen equipment operation and maintenance costs	s_{yw}^{ASO}	0.05	KW
Carbon capture equipment operation and maintenance costs	s_{yw}^{CCE}	0.05	CNY/KWh
Gas unit operation and maintenance costs	s_{yw}^{GU}	0.02	CNY/KWh
Oxygen storage tank operation and maintenance costs	s_{yw}^{OT}	0.05	CNY/m^3
Upper limit of the power consumption of the air oxygen generator	P_{max}^{ASO}	400	KW
Carbon capture equipment baseline energy consumption	P_B^{OCC}	50	KW

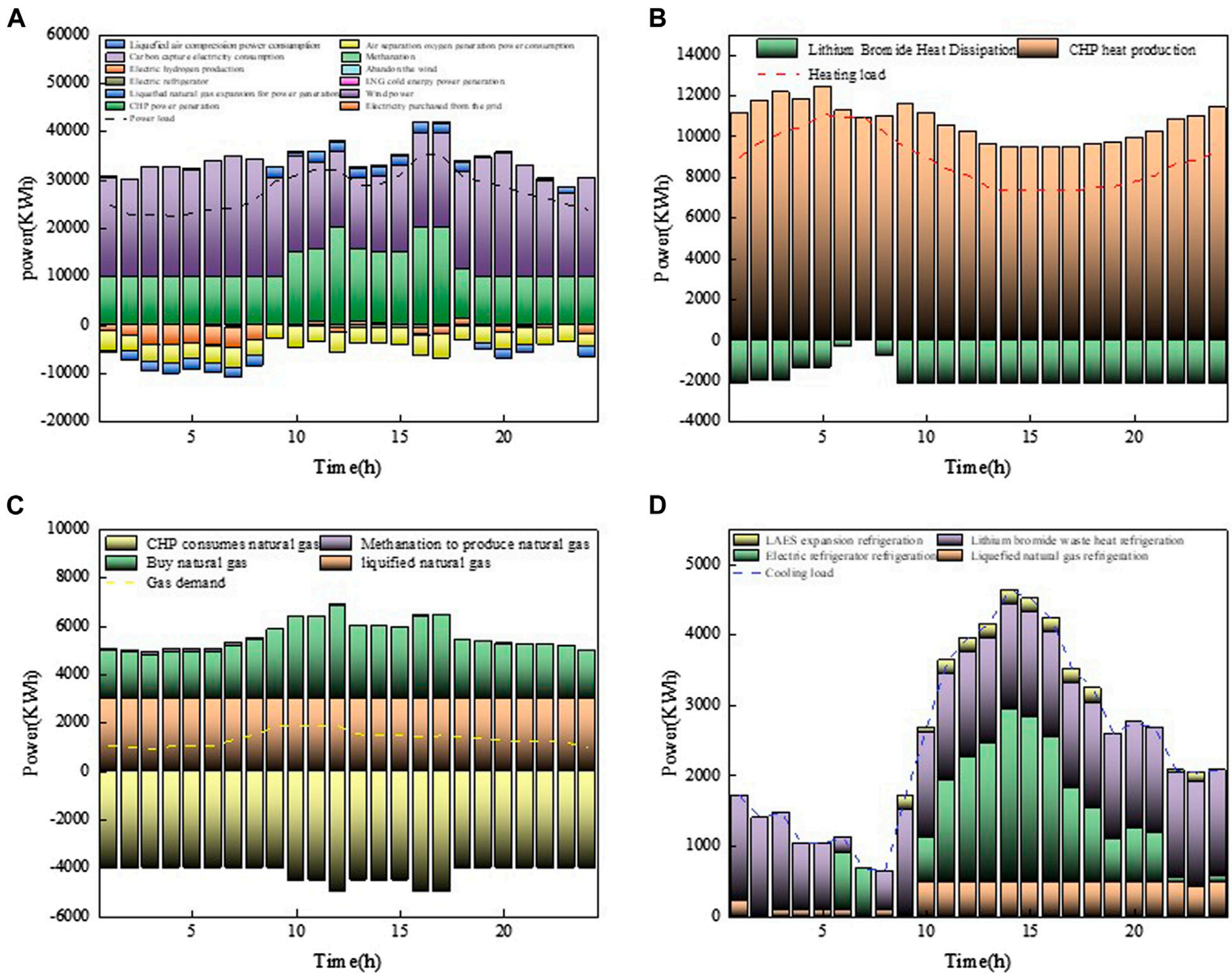

FIGURE 7
Power balance diagram of the integrated energy system.

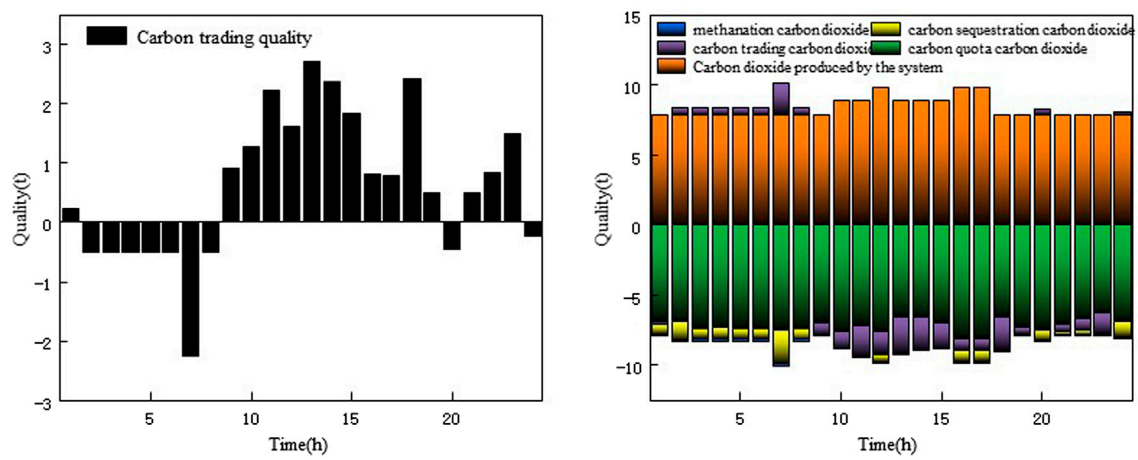

FIGURE 8
Carbon dioxide emissions from integrated energy systems.

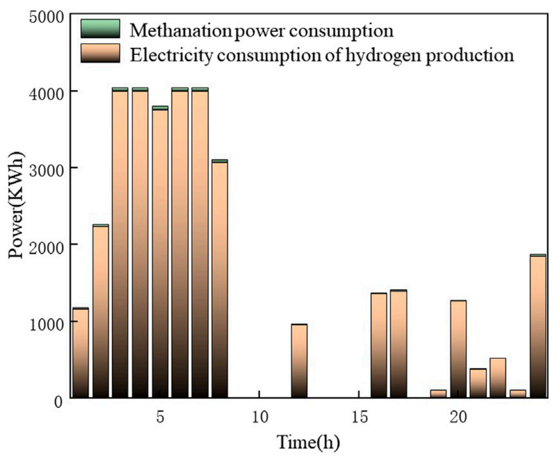

FIGURE 9
Power-to-gas (P2G) device operation results.

6 Example analyses

6.1 Parameters of the algorithm

The structure of the algorithm is shown in Figure 1. The carbon emission intensity of the gas turbine is 1.964 kg/m^3, the climbing rate is 10,000 kW/h, and the operation and maintenance cost is 0.02 yuan/KW; the maximum storage/discharge rate and efficiency of the oxygen storage tank are 2,500 m^3/h and 95%, respectively, the maximum oxygen storage capacity is 10,000 m^3/h, the dissipation coefficient is 0.02%, and the operation and maintenance coefficient is 0.02 yuan/m^3; the base price of carbon emission is taken as 200 CNY/ton, the interval length is taken as 2t, and the growth rate is taken as 0.25; the operation and maintenance cost of the P2G equipment is taken as 0.02 yuan/kWh; the penalty for wind abandonment of wind power is 0.6 CNY/KWh, and the operation and maintenance cost is 0.2 yuan/kWh; and the cost of the load loss penalty is 10 CNY/kWh. Figure 6 shows the power load prediction curve of the IES, which contains the power of each load and the predicted power of wind power. Table 1 shows the time-of-use electricity price and time-of-use natural gas price; Table 2 shows the parameters of the IES equipment; Table 3 shows the basic parameters of oxygen-rich combustion capture technology. In the calculation analysis, t means the time period of t in the scheduling day. For example, when t = 1, it means the first scheduling time period of the day.

6.2 Analysis of basic operational results

In order to verify that the proposed strategy can satisfy the system supply and demand balance, the operational results obtained from the proposed model are analyzed.

TABLE 4 Settings of different scenarios.

Scenario	Demand response	Oxygen-rich combustion capture technology	P2G residual heat and pure oxygen recovery
1	-	-	-
2	√	-	-
3	√	√	-
4	√	√	√

TABLE 5 Operation strategy in different scenarios.

Operating data	Scenario 1	Scenario 2	Scenario 3	Scenario 4
Total costs	495,488	473,738	464,390	463,581
Natural gas purchase costs	458,865	429,967	419,580	418,869
Power purchase costs	1,158	1,801	1,603	1,903
Operation and maintenance (O&M) costs	29,887	36,860	37,750	37,807
Carbon trading costs	5,578	4,125	3,105	2,669
Carbon sequestration costs	0	0	1,302	1,275
Carbon sequestration costs	0	985	1,005	1,058
Carbon emissions	330	260	198	184

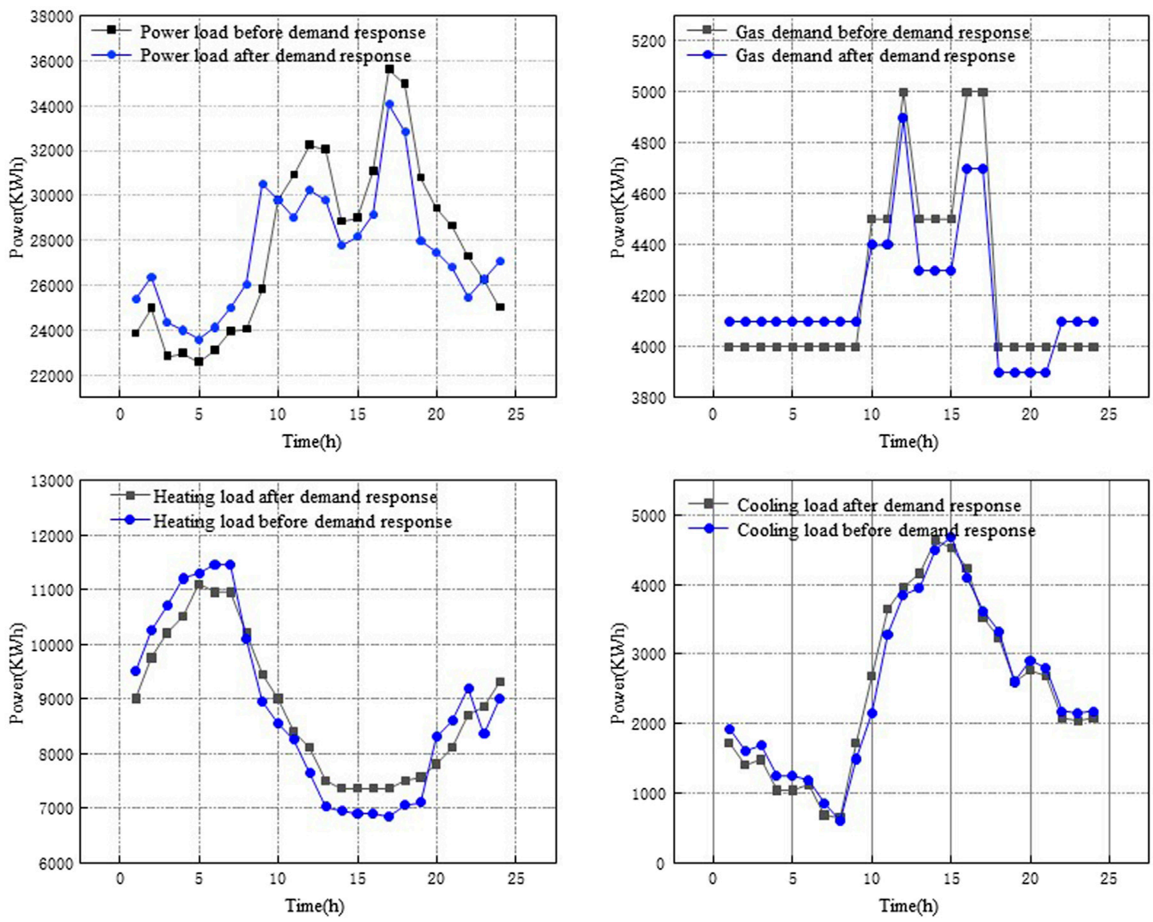

FIGURE 10
Load comparison and after integrated energy system demand response.

Figure 7A shows that the IES only purchases electricity from the grid at the time periods of T = 11, 13, 14, and 18, and the electric load at other times mainly comes from the oxygen-rich combustion capture unit and wind power, which indicates that the IES has high self-sufficiency in electric energy. Figure 7B shows that the residual heat from the reaction of the oxygen-rich combustion unit and the P2G equipment can meet the system heat load. Figure 7C shows that the gas load mainly consists of the upper gas network, liquefied natural gas, and natural gas produced by machination, which can meet the gas turbine and system gas load. Similarly, Figure 7D shows that the output of each unit in the system can meet the system cooling load.

10.3389/fenrg.2024.1296709

TABLE 6 Oxygen blending ratio and oxygen consumption of air separation oxygen generation in scenario 4.

Scenario	Oxygen generation equipment for oxygen production	Power-to-gas (P2G) oxygen supply	Net output of the gas turbine unit	Total output of the gas turbine unit
3	234,643.59	0	288,072.56	32589.21
4	229,861.67	10,011.98	289,560.21	33451.78

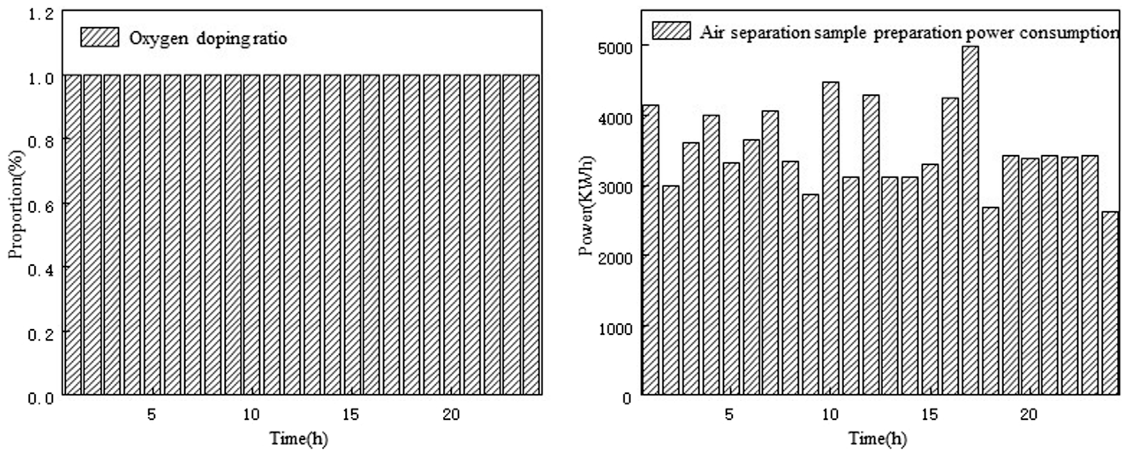

FIGURE 11
Air separation oxygen generation unit operation.

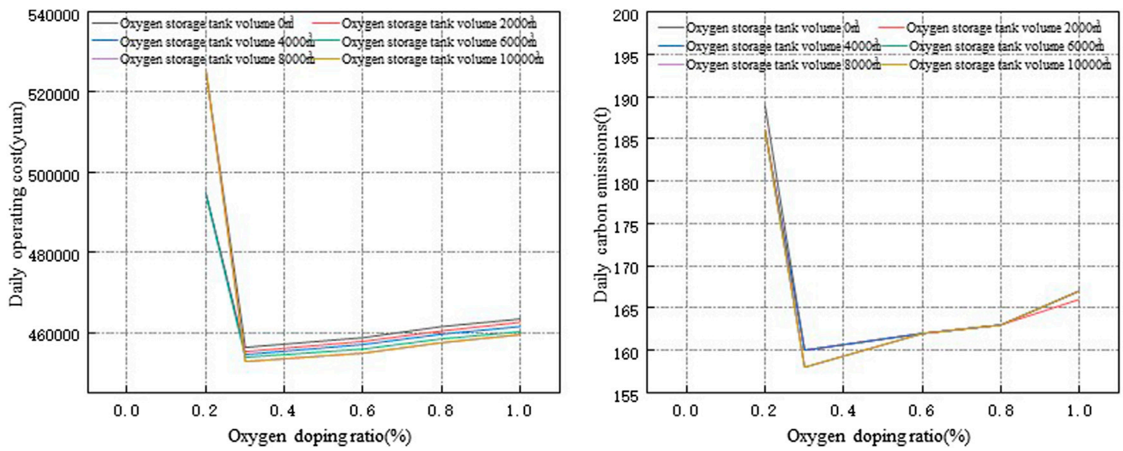

FIGURE 12
Capacity of the oxygen storage tank and oxygen mixing ratio of the oxygen storage tank.

Figure 8 shows that most of the CO_2 generated by the IES is sequestered after the carbon quota, while the other part is used as raw material for the reaction of the P2G equipment, which reduces the cost of carbon trading. In addition, the natural gas generated from it can be used as a raw material for gas turbine units, achieving internal carbon resource circulation and improving the clean efficiency of system operation.

Figure 9 shows that the higher electric power consumption of the P2G equipment at night reduces the wind loss caused by the reverse peaking characteristic of wind power, and the total amount of methane generated by the equipment accounts for approximately 6.05% of the total consumption of the system, which, to a certain extent, reduces the dependence of the system on the external gas source, improves the internal energy conversion capability of the system, and further improves the carbon trading revenue of the system due to the carbon reduction characteristic of the system itself. In addition, the amount of the residual heat heating volume of the P2G equipment accounts for approximately 1.57% of the total heat energy demand, indicating that the P2G equipment also shows certain heating potential. Thus, the P2G equipment has manifold

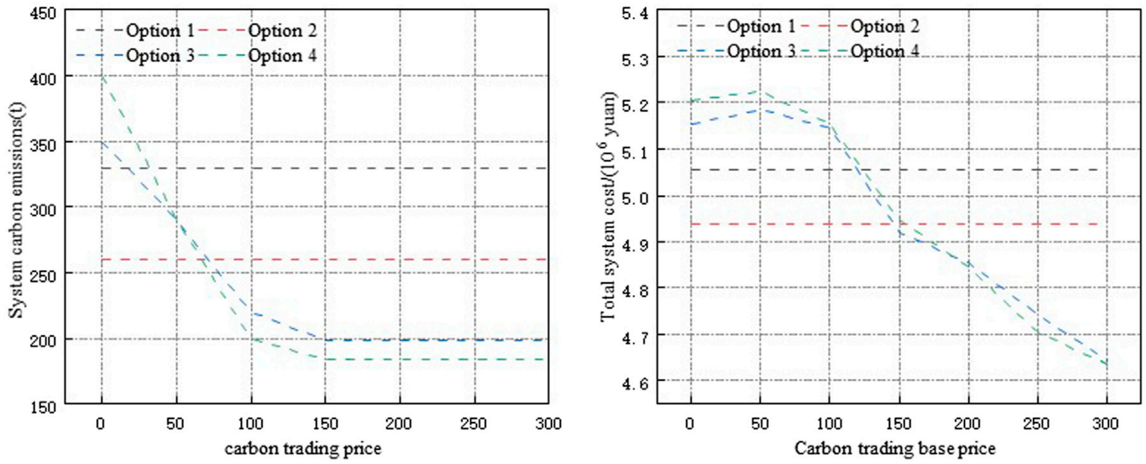

FIGURE 13
Analysis of the impact of the carbon trading base price on operating costs and carbon emissions.

potentials, which can effectively improve the operational flexibility and economic revenues of the system.

6.3 Effectiveness analysis of the operational strategies

In order to verify the effectiveness of the proposed strategy, four different operational scenarios are set up for comparison and verification, and details of the scenarios are shown in Table 4.

Table 5 shows that the carbon emission and total cost of scenario 2 are higher than those of scenario 1, indicating that the demand response can change the energy use habits of users on the load side, promote the consumption of wind power, and improve the economy and low-carbon of the IES. The carbon transaction cost and carbon emissions of scenarios 3 and 4 are much better than those of scenarios 1 and 2, indicating that the introduction of oxygen-rich combustion capture technology and demand response technology not only reduces the carbon emissions of the system to obtain higher economic benefits but also improves the flexibility of the system and reduces the amount of the system wind abandonment.

Figure 10 shows that the electricity, gas, heat, and cooling loads change in scenarios 2 and 3 before and after introducing the demand response and oxygen-rich combustion capture technology. Under the guidance of time-of-use pricing, the electric and gas loads are transferred from the peak period of energy consumption to the valley period, achieving the effect of load “peak shaving and valley filling.” On the other hand, the cooling and heat loads are reasonably adjusted within the comfort level according to the indoor temperature, water temperature changes, and external heat disturbance factors, and certain adjustment incentive subsidies are provided. For electricity and gas loads, after considering the incentive-based IDR, different reductions occur during the later time periods of electricity and gas consumption, respectively. After the introduction of oxygen-rich combustion capture technology and demand response technology, the electricity load is guided by the time-of-use electricity price to transfer to the peak period of the wind power output. The oxygen-rich combustion capture technology regulates the output of gas units in the IES, and the proportion of clean energy increases significantly, indicating that the power supply capacity within the system has increased. In addition, the carbon emissions have been reduced significantly so as to realize the low-carbon and economic operation of the IES.

Combined with Table 6 and Figure 11, it can be seen that in the time period from 5 to 10 o’clock, the power consumption of the air separation oxygen generation equipment in scenario 4 is significantly lower than that in scenario 3, and the oxygen supply of the P2G equipment in scenario 4 accounts for approximately 4.17% of the total oxygen generation of the system, which effectively reduces the oxygen consumption of the gas turbine. Moreover, the gas turbine output of scenario 4 accounts for approximately 75.55% of the total output of the turbine, which is approximately 2.1% higher than that of scenario 3, which shows that the oxygen recovery of the power conversion equipment can effectively reduce the oxygen consumption, improve the net output level of the gas turbine, and reduce the operating cost of the integrated energy system.

In summary, this strategy can improve the output level of the system units, improve the consumption of wind power, tap the operating potential of the P2G equipment and the oxygen equipment, and take into account the low-carbon and economic operation of the system, which verifies the effectiveness of this strategy in the low-carbon and economic operation of the IES.

6.4 Capacity configuration analysis of the air separation oxygen generation equipment and oxygen storage tank

Figure 12 shows that the change trend of the total cost of the system first decreases and then increases with the capacity increase of the oxygen storage tank and air separation oxygen generation equipment, and there is a minimum point (30%, 10,000, 454370.14).

The reason is that with the increase in the capacity of the oxygen storage tank and air separation oxygen generation equipment, the maintenance cost of the equipment gradually increases, but the carbon capture volume is also in the upward trend. The oxygen storage tank capacity has little effect on the carbon emission, while air separation capacity has a greater effect on it, and the overall trend of the carbon emission is to decrease with the increase in air separation capacity. In addition, the trend levels are off after 10,000 m^3 because the capacity of the installed 1-MW thermal power unit requires up to 10,000 m^3/h oxygen.

6.5 Analysis of the carbon trading price

With the proposal of the "dual-carbon" goal, low-carbon emission has become a development trend, and carbon trading prices have changed accordingly. Different carbon trading prices are analyzed in this article, and the analysis of the system economy and low-carbon emission under four options is conducted, which proves the rationality of introducing demand response and oxygen-rich combustion units.

Figure 13 shows that the costs of option 1 and option 2 have been continuously increasing, and the capture of oxygen-rich combustion first increases and then decreases after combustion. The reason is that with the increase in carbon trading, oxygen-rich combustion capture units after combustion can do carbon capture and obtain profits. The reason for the high cost of oxygen-rich combustion units at 10–50 CNY/t is that the oxygen generation unit and P2G equipment produce oxygen at low-carbon trading prices but do not consume carbon dioxide. The oxygen-rich combustion capture units start to do the carbon capture when the carbon trading price is over 50 CNY/t, resulting in a decrease in the cost. When the carbon trading price is 120 CNY/t, the system cost of oxygen-rich combustion power plants is lower than that of conventional power plants, while the system cost capture of power plants after combustion are not lower than that of conventional power plants, proving the economic advantages of oxygen-rich combustion power plants. The P2G equipment in option 4 consumes a portion of CO_2, resulting in a lower carbon trading price than that in option 3.

It can be seen that in most cases, the carbon emissions of the oxygen-rich combustion power plant system are lower than that of the post-combustion capture power plant. The reason for the high carbon trading price of 10–50 CNY/t is that they have not undergone carbon capture, and the oxygen-rich combustion power plant also needs to supply air separation and oxygen production facilities for operation, consuming additional electricity and generating additional CO_2. When the carbon trading price is 30 CNY/t, the carbon emissions of the oxygen-rich combustion power plant system decrease first compared to the post-combustion capture system, and there is more room for the decrease, proving the advantages of oxygen-rich combustion power plants in carbon capture.

7 Conclusion

This article introduces the oxygen-rich combustion capture unit and demand response into the IES, considering the residual heat recovery and oxygen utilization of the P2G equipment. In addition, an IES operation optimization method considering carbon trading efficiency is proposed. The following conclusions can be drawn through the example analysis:

1. The introduction of oxygen-rich combustion capture technology and demand response can meet the multi-energy requirements within the system, achieve the bi-directional conversion of multiple energies, improve the operational flexibility of the system, and have good carbon reduction effects and economic efficiency.
2. The capacity of the air separation oxygen generation equipment and oxygen storage tank has the most cost advantage. However, at this time, the carbon emissions are not optimal and need to be configured according to the actual situation.
3. Under the action of the integrated demand response, the IES has achieved the effect of load "peak shaving and valley filling," with a significant increase in the proportion of clean energy and an increase in the output of low-carbon units within the system, improving the low-carbon and economic efficiency of the IES.
4. By comparing the costs and carbon emissions under different carbon trading prices, it has been proven that the scheduling scheme of the oxygen-rich combustion power plant system can achieve the optimal effect in terms of economy and low-carbon performance.

Data availability statement

The raw data supporting the conclusion of this article will be made available by the authors, without undue reservation.

Author contributions

XJ: writing–review and editing, project administration, methodology, and conceptualization. LMn: writing–review and editing, methodology, and conceptualization. LMi: writing–original draft, methodology, and conceptualization. HH: writing–review and editing and formal analysis.

Funding

The author(s) declare that financial support was received for the research, authorship, and/or publication of this article. This work was supported by "Land Scenery Three Gorges" High-Quality Development Major Science and Technology Project-Park-Level Multi-Micro-Grid System, Jilin Province, participating in key technology research projects for grid-friendly interaction (No. 20230303003SF).

Conflict of interest

The authors declare that the research was conducted in the absence of any commercial or financial relationships that could be construed as a potential conflict of interest.

Publisher's note

All claims expressed in this article are solely those of the authors and do not necessarily represent those of their affiliated organizations, or those of the publisher, the editors, and the reviewers. Any product that may be evaluated in this article, or claim that may be made by its manufacturer, is not guaranteed or endorsed by the publisher.

References

Chrispim, M. C. (2021). Resource recovery from wastewater treatment: challenges, opportunities and guidance for planning and implementation. *Front. Neurosci.* 14 (1).

Cui, Y., et al. (2021). Low-carbon economic dispatch of electro-gas-thermal integrated energy system based on oxy-combustion technology. *Zhongguo Dianji Gongcheng Xuebao/Proceedings Chin. Soc. Electr. Eng.* 41 (2). doi:10.13334/j.0258-8013.pcsee.191708

Cui, Y., et al. (2022). Multi-time scale source-load dispatch method of power system with wind power considering low-carbon characteristics of carbon capture power plant. *Zhongguo Dianji Gongcheng Xuebao/Proceedings Chin. Soc. Electr. Eng.* 42 (16). doi:10.13334/j.0258-8013.pcsee.210697

Dai, K., Zhang, K., Li, J., Liu, L., Chen, Z., and Sun, P. (2023). Low-carbon optimal scheduling model for peak shaving resources in multi-energy power systems considering large-scale access for electric vehicles. *Processes* 11 (5), 1532. doi:10.3390/pr11051532

Gao, D., et al. (2014). Flue gas dynamic characteristics and operation economic analysis of oxy-fuel combustion circulating fluidized bed boiler. *Zhongguo Dianji Gongcheng Xuebao/Proceedings Chin. Soc. Electr. Eng.* 34. doi:10.13334/j.0258-8013.pcsee.2014.S.016

Gao, D., et al. (2019). Influence factor analysis of circulating fluidized bed boiler oxy-fuel combustion and CO2 capture power generation unit operation energy consumption. *Zhongguo Dianji Gongcheng Xuebao/Proceedings Chin. Soc. Electr. Eng.* 39 (5). doi:10.13334/j.0258-8013.pcsee.180505

Guan, Y., Han, Y., Wu, M., Liu, W., Cai, L., Yang, Y., et al. (2018). Simulation study on the carbon capture system applying LNG cold energy to the O2/H2O oxy-fuel combustion. *Nat. Gas. Ind. B* 5 (3), 270–275. doi:10.1016/j.ngib.2017.11.011

Guo, Z., and Zhou, S. (2023). Modeling and multi-stage planning of cement-IIES considering carbon-green certificate trading. *Processes* 11 (4), 1219. doi:10.3390/pr11041219

Han, X., et al. (2021). New issues and key technologies of new power system planning under double carbon goals. *Gaodianya Jishu/High Volt. Eng.* 47 (9). doi:10.13336/j.1003-6520.hve.20210809

He, L., Liao, C., and Tjong, S. C. (2018). Scalable fabrication of high-performance transparent conductors using graphene oxide-stabilized single-walled carbon nanotube inks. *Appl. Energy* 8, 224. doi:10.3390/nano8040224

Ji, X., et al. (2022). Coordinated optimal dispatch of transmission and distribution power systems considering operation flexibility of integrated energy system. *Dianli Xit. Zidonghua/Automation Electr. Power Syst.* 46 (23). doi:10.7500/AEPS20220215008

Kang, L., et al. (2022). Low-carbon economic dispatch of integrated energy system containing LNG cold energy utilization. *Gaodianya Jishu/High Volt. Eng.* 48 (2). doi:10.13334/j.0258-8013.pcsee.2010.s1.028

Koiwanit, J., Manuilova, A., Chan, C., Wilson, M., and Tontiwachwuthikul, P. (2014). A life cycle assessment study of a hypothetical Canadian oxy-fuel combustion carbon dioxide capture process. *Int. J. Greenh. Gas Control* 28, 257–274. doi:10.1016/j.ijggc.2014.07.001

Liang, Z., Mu, L., and He, C. (2021). Robust optimal dispatch of interconnected micro-energy network based on cooperative game. *J. Renew. Sustain. Energy* 13 (4). doi:10.1063/5.0051157

Liu, Y., Zhu, L., and Yan, W. (2010). Economic assessment for the CO2 capture technologies applied in the coal-firing power plant. *Zhongguo Dianji Gongcheng Xuebao/Proceedings Chin. Soc. Electr. Eng.* 30. SUPPL. doi:10.13336/j.1003-6520.hve.20201844

Lu, Z., et al. (2018). Low-carbon economic dispatch of the integrated electrical and heating systems based on benders decomposition. *Zhongguo Dianji Gongcheng Xuebao/Proceedings Chin. Soc. Electr. Eng.* 38 (7). doi:10.13334/j.0258-8013.pcsee.2010.s1.028

Malehmirchegini, L., and Farzaneh, H. (2022). Demand response modeling in a day-ahead wholesale electricity market in Japan, considering the impact of customer risk aversion and dynamic price elasticity of demand. *Energy Rep.* 8, 11910–11926. doi:10.1016/j.egyr.2022.09.027

Masoud, M., Siamak, H., and Astiaso, D. G. (2024). Developing particle-based models to predict solar energy attenuation using long-term daily remote and local measurements. *J. Clean. Prod.*, 434139690. doi:10.13334/j.0258-8013.pcsee.171058

Masoud, N., Laureano, J., et al. (2023). Carbon footprint of low-energy buildings in the United Kingdom: effects of mitigating technological pathways and decarbonization strategies. *Sci. total Environ.*, 882163490–163490. doi:10.1016/j.jclepro.2023.139690

Oboirien, B. O., North, B. C., and Kleyn, T. (2014). Techno-economic assessments of oxy-fuel technology for South African coal-fired power stations. *Energy* 66, 550–555. doi:10.1016/j.energy.2013.12.032

Qin, T., et al. (2018). Carbon trading based low-carbon economic dispatch for integrated electricity-heat-gas energy system. *Dianli Xit. Zidonghua/Automation Electr. Power Syst.* 42 (14). doi:10.1016/j.energy.2013.12.032

Siamak, H., Daniele, G., Scarlet, A. S., Di Matteo, U., and Astiaso Garcia, D. (2022). The PRISMI plus toolkit application to a grid-connected mediterranean island. *Energies* 15 (22), 8652. doi:10.3390/en15228652

Siamak, H., Davide, G. A., and Lizhen, H. (2023). Grid-connected renewable energy systems flexibility in Norway islands' Decarbonization. *Renew. Sustain. Energy Rev.*, 185.

Tian, N. J., et al. (2023). Optimization method for medium and long term dispatch schedule considering schedule execution and new energy consumption. *Shenyang Gongye Daxue Xuebao/Journal Shenyang Univ. Technol.* 45 (2). doi:10.3390/EN15228652

Wang, Z., et al. (2019). Low carbon economy operation and energy efficiency analysis of integrated energy systems considering LCA energy chain and carbon trading mechanism. *Zhongguo Dianji Gongcheng Xuebao/Proceedings Chin. Soc. Electr. Eng.* 39 (6). doi:10.13334/j.0258-8013.pcsee.180754

Yang, D., et al. (2022). Economic-emission dispatch problem in integrated electricity and heat system considering multi-energy demand response and carbon capture Technologies. *Energy*, 253. doi:10.1016/J.ENERGY.2022.124153

Zaharia, A., Diaconeasa, M. C., Brad, L., Lădaru, G. R., and Ioanăș, C. (2019). Factors influencing energy consumption in the context of sustainable development. *Sustain. Switz.* 11 (15), 4147. doi:10.3390/su11154147

Zhang, D., et al. (2022). Operational optimization of integrated cooling, heating and power energy system considering concentrating solar power plant and heat balance of building. *Gaodianya Jishu/High Volt. Eng.* 48 (7).

Zhang, T., She, X., and Ding, Y. (2021). A power plant for integrated waste energy recovery from liquid air energy storage and liquefied natural gas. *Chin. J. Chem. Eng.* 34, 242–257. doi:10.1016/j.cjche.2021.02.008

Zhou, R., et al. (2018). Coordinated optimization of carbon utilization between power-to-gas renewable energy accommodation and carbon capture power plant. *Dianli Zidonghua Shebei/Electric Power Autom. Equip.* 38 (7).

Zhu, Z., Sheng, M., and Chen, Z. (2022). Low-carbon economic dispatching of integrated energy system considering liquid air energy storage and integrated demand response. *Dianli Zidonghua Shebei/Electric Power Autom. Equip.* 42 (12). doi:10.16081/j.epae.202210003